Pressure-induced phase transition in $BaCrO_4$

Tony Huang,[1] Sean R. Shieh,[2] Arslan Akhmetov,[2] Xi Liu,[3] Chih-Ming Lin,[4] and Jiann-Shing Lee[5]
[1]*Department of Earth Sciences, National Cheng Kung University, Tainan 701, Taiwan*
[2]*Department of Earth Sciences, University of Western Ontario, London, ON, Canada N6A 5B7*
[3]*School of Earth and Space Science, Peking University, Beijing 100871, People's Republic of China*
[4]*Department of Applied Science, National Hsinchu University of Education, Hsinchu 300, Taiwan*
[5]*Department of Applied Physics, National Pingtung University of Education, Pingtung 900, Taiwan*
(Received 17 June 2009; revised manuscript received 6 May 2010; published 22 June 2010)

$BaCrO_4$ was studied to 25 GPa in a diamond-anvil cell using both Raman spectroscopy and x-ray diffraction methods. Our results showed that $BaCrO_4$ exhibits a phase transition near 9 GPa from both Raman and x-ray diffraction measurements. The new high-pressure phase ($BaCrO_4$-II) is suggested as a monoclinic ($P2_1/m$) structure, different from other high-pressure forms of ABO_4-type compounds. Moreover, the high-pressure phase of $BaCrO_4$ is found to be reversible; the low-pressure phase is recovered at ~8 GPa upon decompression. The pressure-volume data of $BaCrO_4$ fitted to a third-order Birch-Murnaghan equation of state yield a bulk modulus of 53(1) GPa and a pressure derivative of 6.8(5), in agreement with the theoretical prediction. For the high-pressure phase $BaCrO_4$-II, the bulk modulus is 117(10) GPa and the pressure derivative is 3(1).

DOI: 10.1103/PhysRevB.81.214117 PACS number(s): 62.50.−p, 61.50.−f, 81.40.Vw

I. INTRODUCTION

$A^{2+}B^{6+}O_4^{2-}$-type compounds in barite, monazite, zircon, and scheelite structures are of great interest in Earth Science,[1] Material Science,[2–4] and Physics.[5] The coordination numbers of A and B cations in compounds $A^{2+}B^{6+}O_4^{2-}$ vary with pressure and chemical composition; a systematic trend within some compounds was reported.[6–8] Recently, an updated north-east phase-transition trend for a great number of ABX_4 compounds (i.e., Bastide's diagram) has been reported by Errandonea *et al.*[9] The updated Bastide's diagram is based on the ratios of cation-to-anion radii which are r_B/r_x vs r_A/r_x. In such a trend, the high pressure forms of the ABO_4 compounds located at the lower right region of the diagram with low r_B/r_x and high r_A/r_x become difficult to predict. Barium chromate ($BaCrO_4$) is one of the ABO_4-type compounds that locate at lower right area of the Bastide's diagram and thus little is known about its high-pressure form. $BaCrO_4$ is isostructural with barite ($BaSO_4$), having orthorhombic symmetry with space group *Pnma* (No. 62, $Z=4$).[10] In the orthorhombic structure of $BaCrO_4$ [Fig. 1(a)], the Cr^{6+} ions are tetrahedrally coordinated by oxygen; the sites between isolated CrO_4 tetrahedral units are occupied by Ba^{2+} ions and the Ba^{2+} ions are eightfold coordinated with oxygen [Fig. 1(b)]. A high-pressure phase of $BaSO_4$ has been reported at above 9 GPa but its structure remains unresolved.[11] Furthermore, the transition pressure of $BaSO_4$ observed from Raman and x-ray diffraction is also inconsistent.[11]

Moreover, Hazen *et al.*[12,13] suggested an equation for the bulk modulus which exhibits inverse proportionality to the bond length, between the A cation and oxygen of ABO_4 compounds, and Errandonea *et al.*[9,14] modified the equation from Hazen. The former equation[12,13] was applied to various salts and the latter[9,14] was suited to compounds of scheelite structure. To apply the equation to $BaCrO_4$ requires the knowledge of bulk modulus of $BaCrO_4$. However, the availability of the bulk modulus of $BaCrO_4$ is limited to the theoretical prediction.[15] Therefore, it is important to obtain the reliable bulk modulus of $BaCrO_4$ and to examine availability of the equation proposed by Hazen *et al.*[12,13] and Errandonea *et al.*[9,14] for $BaCrO_4$. In this study, we investigate $BaCrO_4$ at high pressures using both x-ray diffraction and Raman spec-

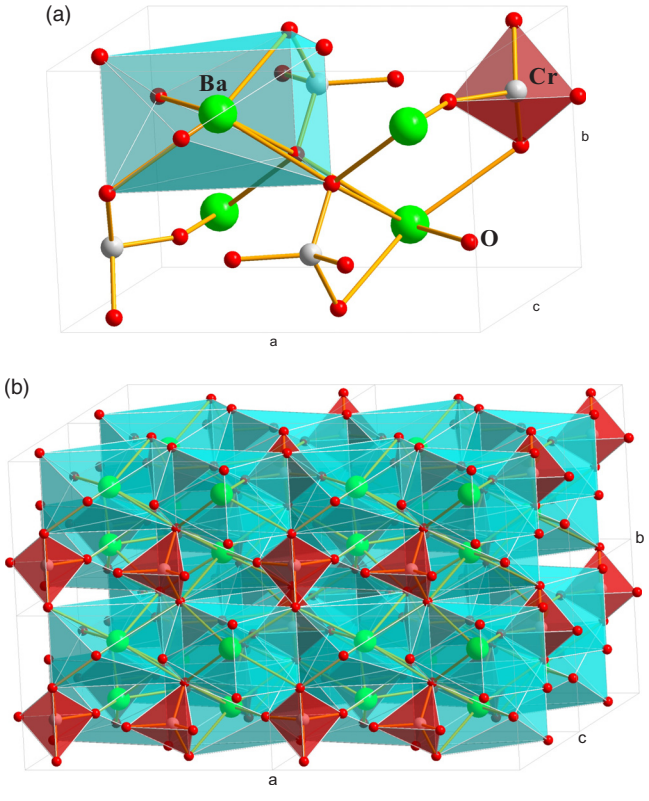

FIG. 1. (Color online) Barite structure of $BaCrO_4$: large circles represent Ba atoms, medium circles represent Cr atoms, and small circles represent O atoms. (a) BaO_8 polyhedron and CrO_4 tetrahedron. (b) BaO_8 polyhedron edge shared along a axis, the least compressible direction.

troscopy, report the bulk modulus, and present the discovery of a high-pressure form of $BaCrO_4$.

II. EXPERIMENTS

$BaCrO_4$ was synthesized by chemical reaction of $BaCl_2$ and Na_2CrO_4 at 1050 °C.[16] Examination of the synthesized $BaCrO_4$ with electron-probe microanalysis confirmed its chemical composition and with conventional x-ray diffraction confirmed its structure. The x-ray diffraction result showed that the starting material is a pure $BaCrO_4$, with unit-cell parameters $a=9.106(1)$ Å, $b=5.539(1)$ Å, and $c=7.335(1)$ Å at 298 K. In this study, a diamond-anvil cell was used for x-ray diffraction and Raman-scattering measurements. The starting material was loaded into a stainless-steel gasket with a hole of 150 μm in diameter, together with a 4:1 methanol-ethanol mixture as a pressure-transmitting medium, which ensured satisfactory hydrostatic conditions up to 11 GPa.[17] This sample configuration was applied to both x-ray diffraction and Raman measurements. For x-ray diffraction measurements, pressure was measured by gold powder[18] loaded with the sample while in Raman-scattering measurements pressure was determined by the ruby fluorescence method.[19]

In situ high-pressure x-ray diffraction was performed at beamline X17C, National Synchrotron Light Source at Brookhaven National Laboratory; a monochromatic x-ray beam of wavelength 0.4066 Å served as the probing source. Two-dimensional images of x-ray diffraction were collected with an imaging plate detector. CeO_2 served to calibrate both the distance from sample to detector and the orientation of the detector. Each image was collected for about 10 min. Program FIT2D (Ref. 20) was used to deduce the two-dimensional images into one-dimensional x-ray diffraction patterns. PEAK-FITTING and GSAS programs produced the lattice parameters and volumes of the samples.[21]

Ruby fluorescence and Raman spectra were performed in a micro-Raman system (TRIAX 550 Jobin–Yvon Spex) and recorded with a spectrometer equipped with a charge coupled device detector cooled with liquid nitrogen; an argon-ion laser (wavelength of 514.5 nm, output power of 0.6 W) served for excitation source. The precision in the frequency determination of this micro-Raman system was about 1 cm^{-1}. For ruby fluoresces measurements, the corresponding error of pressure was within $\pm 0.1-0.2$ GPa at the greatest pressure because a satisfactory ratio of signal to noise was achieved in the system even for broad lines below 20 GPa. For Raman measurement, the backscattered Raman signals were collected for 5–20 s for each Raman spectrum. A computer program (Jandel Scientific PEAKFIT) was used to fit our Raman lines with Voigt profiles.

III. RESULTS

A. X-ray diffraction results

In situ high-pressure x-ray diffraction patterns of $BaCrO_4$ were recorded to ~25 GPa. Our results showed that three new diffraction peaks appeared at pressure above 9 GPa, indicating a phase transition occurred and consequently they were found to coexist with the original peaks to higher pressures (Fig. 2). However, at pressure above 18 GPa, the features slightly changed and a number of peaks disappeared. This could be due to peak broadening and/or signals weakening at high pressures. Upon decompression, the low-pressure structure was recovered at ~8 GPa, indicating a weak hysteresis. In Fig. 3 *d* spacings is shown as a function of pressure. The phase-transition pressure shows clearly around 9 GPa and more data points are observed for the high-pressure phase.

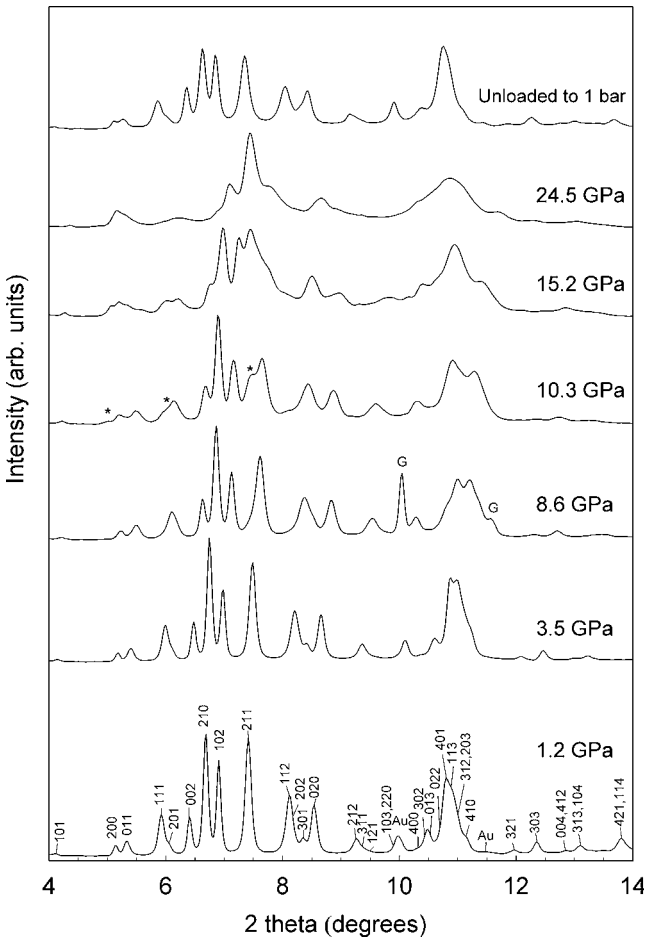

FIG. 2. Representative x-ray diffraction patterns of $BaCrO_4$ at elevated pressures. $BaCrO_4$ exhibited three new features above 9 GPa, marked with ∗. Au denotes gold and G denotes gasket.

B. Raman results

At ambient conditions the Raman spectra of $BaCrO_4$ are shown in Fig. 4. The Raman data show that the lattice modes in the range 90–300 cm^{-1} are ascribed to the motion of the cations and tetrahedron units. The internal modes of vibrations of the CrO_4 tetrahedron spanned the wavenumber range 300–900 cm^{-1} but with a gap between 430 and 860 cm^{-1}. Modes at 800–900 cm^{-1} are associated with stretching vibrations of the tetrahedron whereas those at 300–430 cm^{-1} are assigned to bending vibrations. Our Raman spectrum of $BaCrO_4$ at 1 bar thus includes modes for the lattice (99.2, 114.4, 135.8, 150.1, and 176.4 cm^{-1}), for symmetric stretch-

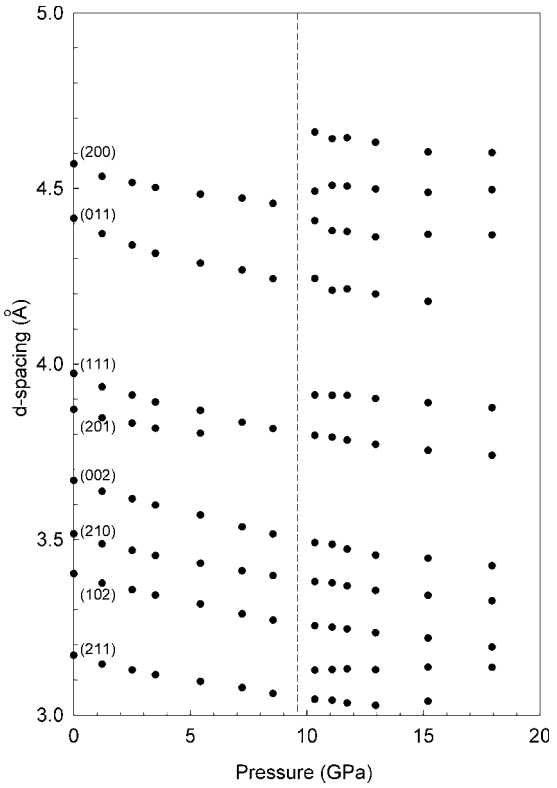

FIG. 3. Variations in d spacings of $BaCrO_4$ under compression. The dashed line indicates the transition pressure.

ing (ν_1=862.0 cm^{-1}), for symmetric bending (ν_2=351.1 and 360.1 cm^{-1}), for antisymmetric stretching (ν_3=872.9 and 898.6 cm^{-1}), and for antisymmetric bending (ν_4=394.5, 406.2, and 430.2 cm^{-1}), in satisfactory agreement with a previous report[22] (Table I).

The Raman spectrum of $BaCrO_4$ was measured to about 20 GPa. Upon compression, a new Raman mode at 891.2 cm^{-1} was observed at about 9 GPa; later two additional modes appeared at 352.1 and 453.2 cm^{-1} at 10.4 GPa [Figs. 4(b) and 4(c)]. Our Raman data thus indicated a new phase to be stable above 9 GPa. Moreover, the intensities of the Raman modes of the initial phase decreased at pressures above 9 GPa. Upon decompression to 1 bar, the Raman modes of the low-pressure form of $BaCrO_4$ were fully retained, indicating the high-pressure form of $BaCrO_4$ to be nonquenchable. The pressure dependences of the observed Raman shifts are shown in Fig. 5. The frequencies of all Raman modes increased with pressure up to about 9 GPa and then a discontinuity is clearly shown at about 9 GPa, indicating a phase transition of $BaCrO_4$. Moreover, four new modes observed above 850 cm^{-1}, a range for internal stretching modes of the new phase, indicating slightly change in the CrO_4 tetrahedral structure.

IV. DISCUSSION

In this section, we discuss first about x-ray results and afterward about Raman results. Figure 6 shows the variations in lattice parameters of the unit cell and the volumes as a function of pressure to 15.1 GPa. Moreover, the linear compressibilities along the three crystallographic axes differ significantly (b axis is about 7.4% more compressible than a axis) and the relative compressibility of three axes showed a result of $\beta_b > \beta_c > \beta_a$ [Fig. 6(a) and Table II]. The volume data of $BaCrO_4$ fitted to a third-order Birch-Murnaghan equation of state yielded a bulk modulus of 53(1) GPa and the pressure derivative of 6.8(5) [Fig. 6(b)]; this value agrees with that from a theoretical calculation, K_0=56.05 GPa (Ref. 15).

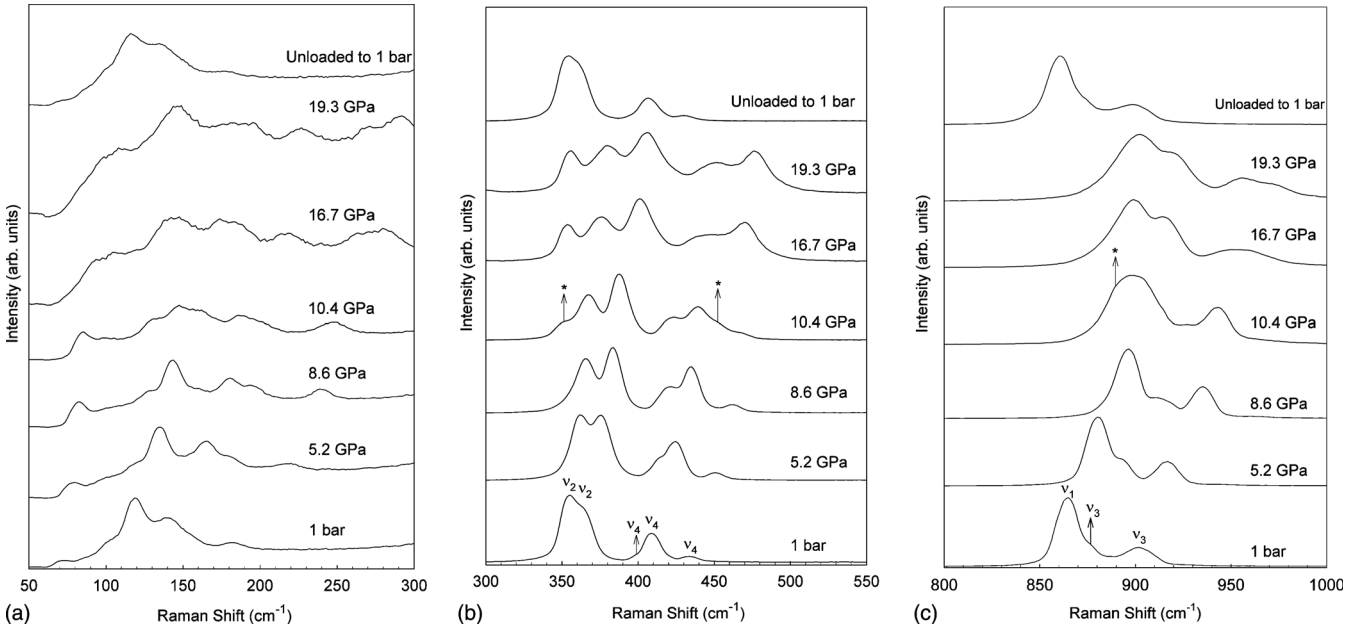

FIG. 4. Representative Raman spectra of $BaCrO_4$ showing the evolution of spectra at elevated pressures and 298 K. $BaCrO_4$ exhibits three new peaks above 9 GPa, marked with ∗. (a) Lattice modes, (b) bending modes, and (c) stretching modes.

TABLE I. Ambient-pressure Raman frequencies, ν_0, their pressure dependences $d\nu/dP$, and mode-Grüneisen parameters γ_0 of $BaCrO_4$.

Vibrational mode	Wavenumber/cm^{-1} Reference 22	Wavenumber/cm^{-1} This work	$d\nu_i/dP$ (cm^{-1}/GPa)	γ_0 [a]
	Internal modes			
ν_3	927.3			
ν_3	906.7			
ν_3	898.4	898.6	4.3	0.25
ν_3	884.2			
ν_3	872.1	872.9	4.7	0.29
ν_1	863	862.0	4.0	0.24
ν_4	427.5	430.2	3.7	0.45
ν_4	411.2			
ν_4	403.3	406.2	3.5	0.46
ν_4	395.1	394.5	3.1	0.42
ν_2	360	360.1	2.7	0.40
ν_2	349.5	351.1	1.6	0.24
	Lattice modes			
	175.4	176.4	7.5	2.25
	146	150.1	5.3	1.87
	135	135.8	5.2	2.02
	122.3			
	112.4	114.4	3.4	1.58
	97.3	99.2	3.4	1.83

[a]Calculated results are based on bulk modulus K_0=53 GPa, obtained from this work.

Besides, when $BaCrO_4$ was subjected to compression, the variation in the bond distance Ba-O in the BaO_8 polyhedron was greater than that of Cr-O in the CrO_4 tetrahedron, according to our XRD data. Our full-profile diffraction data deduced with the GSAS program reveal that the Ba-O bonds are more compressible than those of Cr-O (Fig. 7). As the two longest Ba-O bonds in the $BaCrO_4$ structure tend to align along the *b* axis,[13] despite this axis being the shortest, the *b* axis is thus the most compressible and corresponds to the direction with the greatest Ba-O distance.[23] Figure 1(b) shows the BaO_8 polyhedron edge shared along the *a* axis that is the direction of least compressibility.

Moreover, the bulk modulus of ABO_4-type compounds at high pressure was an important aspect. Hazen and Finger[12] found that the bulk moduli of certain binary oxides and silicates correlate directly with the compressibility of the *A*-cation coordination polyhedron, according to the following equation:

$$K_0 = 750S^2Z_AZ_C/d^3_{A\text{-}O}, \quad (1)$$

where S^2 is the empirical "ionicity" for bond thermal expansivity, Z_A is the valence of the formal charge of the *A* cation, Z_C is the valence of the formal charge of the anion, and $d_{A\text{-}O}$ is the average *A*-O distance/Å inside the polyhedron. S^2 takes values 0.5 for oxides and silicates, 0.4 for sulfides, selenides, and tellurides, 0.25 for phosphates, arsenates, and antimonides, and 0.2 for carbides and nitrides. For chromates, values of S^2 are uncertain. In our $BaCrO_4$ case, we used K_0=53 GPa and 2.838 Å for the mean bond length between barium and oxygen. Our calculation yielded the value S^2=0.40 for $BaCrO_4$. K_0 for $CaCrO_4$ in the zircon structure is 104 GPa,[24] with mean bond length 2.37 Å between calcium and oxygen. Use of Eq. (1) yielded S^2=0.46 for $CaCrO_4$. The mean value of S^2 in the two chromates is 0.43, near the value for sulfides and selenides. Errandonea *et al.*[9,14] suggested a modified relation that is induced by the structure of the compounds, expressed as

$$K = 610Z_A/d^3_{A\text{-}O} \quad (2)$$

This equation was suitable for compounds with scheelite and scheelite-related structures (zircon and barite structures). In terms of the mean Ba-O bond length 2.838 Å, the bulk modulus of $BaCrO_4$ was calculated to be 53 GPa, which agrees reasonably with our experimental results.

The pressure-dependent frequency shifts ($d\nu/dP$) yield the mode-Grüneisen parameters through the equation,

$$\gamma = K_0/\nu_{0i}(d\nu_i/dP) \quad (3)$$

in which K_0 is the bulk modulus and ν_{0i} is the frequency of vibrational mode *i* under ambient conditions. The bulk modulus, K_0=53 GPa, obtained from this study was applied for the calculations. Therefore, the Grüneisen parameters of $BaCrO_4$ were found in the range of 0.29–2.68 (Table I), which lie in two narrow ranges: 0.24–0.46 (internal modes) and 1.58–2.25 (lattice modes). The mean Grüneisen parameter for $BaCrO_4$ is thus calculated to be 0.87. The pressure-dependent frequency shifts, $d\nu_i/dP$, showed the lattice modes (135–175.4 cm^{-1}) generally greater than for those of internal modes. These Raman data support the observations of the bond distances of Ba-O decreased more than those of Cr-O (Fig. 7), hence indicating the BaO_8 polyhedron to be more compressible than the CrO_4 tetrahedron. Moreover, the slopes of frequency shifts of ν_1 and ν_3 modes are slightly greater than those of ν_2 and ν_4 modes at pressures to 8.6 GPa, indicating that the Cr-O stretching modes are more sensitive to pressure than the O-Cr-O bending modes in barite-type $BaCrO_4$ (Fig. 5 and Table I). There is no mode appearance in the phonon gap of the low-pressure and high-pressure phases between 500 and 800 cm^{-1} which indicates the coordination numbers of Cr remaining four in the low- and high-pressure phases.[25] Moreover, there are three and four stretching modes observed in low- and high-pressure phases, respectively. The approximate numbers of stretching modes between low- and high-pressure phases indicate the high-pressure phase structure of $BaCrO_4$ displays tetrahedral coordination of Cr ions.

Weckhuysen and Wachs[26] suggested an empirical formula between the Raman stretching mode frequency (ν) and the Pauling's Cr-O bond strengths (s), expressed as

$$s_{Cr\text{-}O} = [0.3408 \ln(13\,055/\nu)]^{-5} \quad (4)$$

thus it is possible to calculate the coordination of the Cr ion in a chromate compound if we know all the stretching fre-

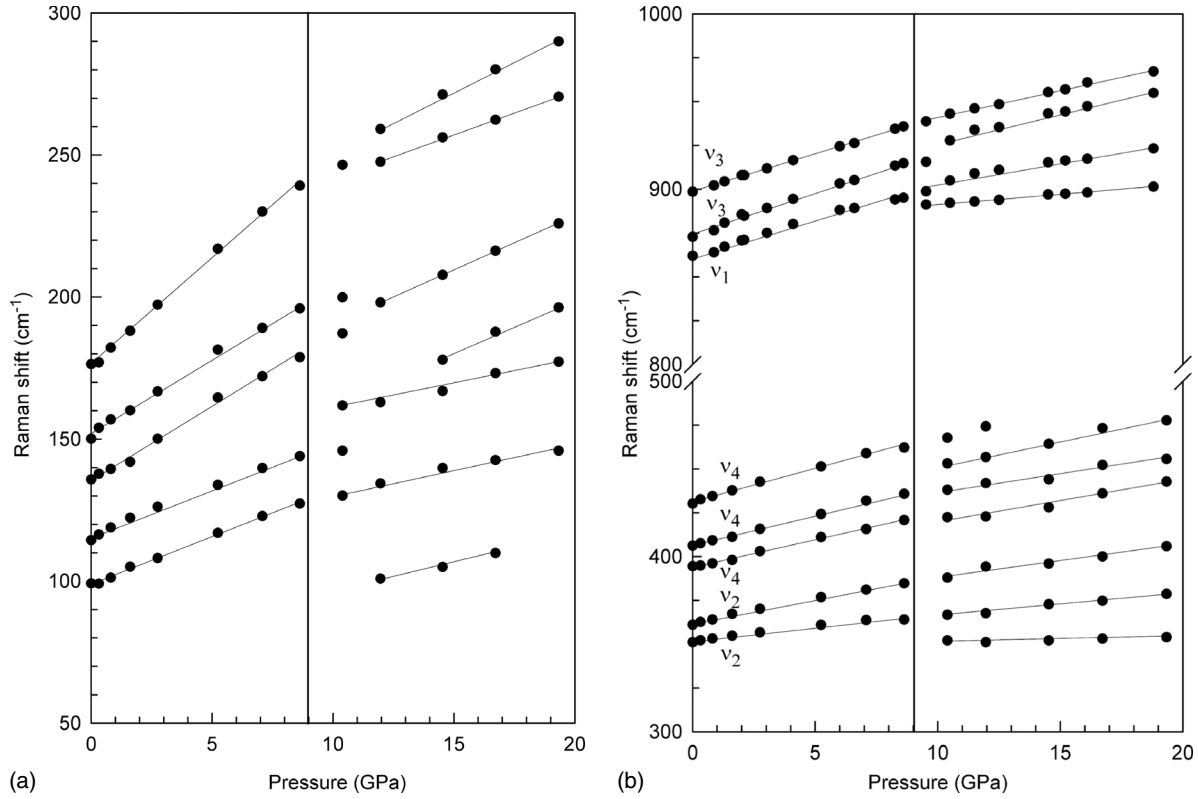

FIG. 5. Frequency shifts of Raman modes of $BaCrO_4$ as a function of pressure. (a) Lattice modes and (b) internal modes.

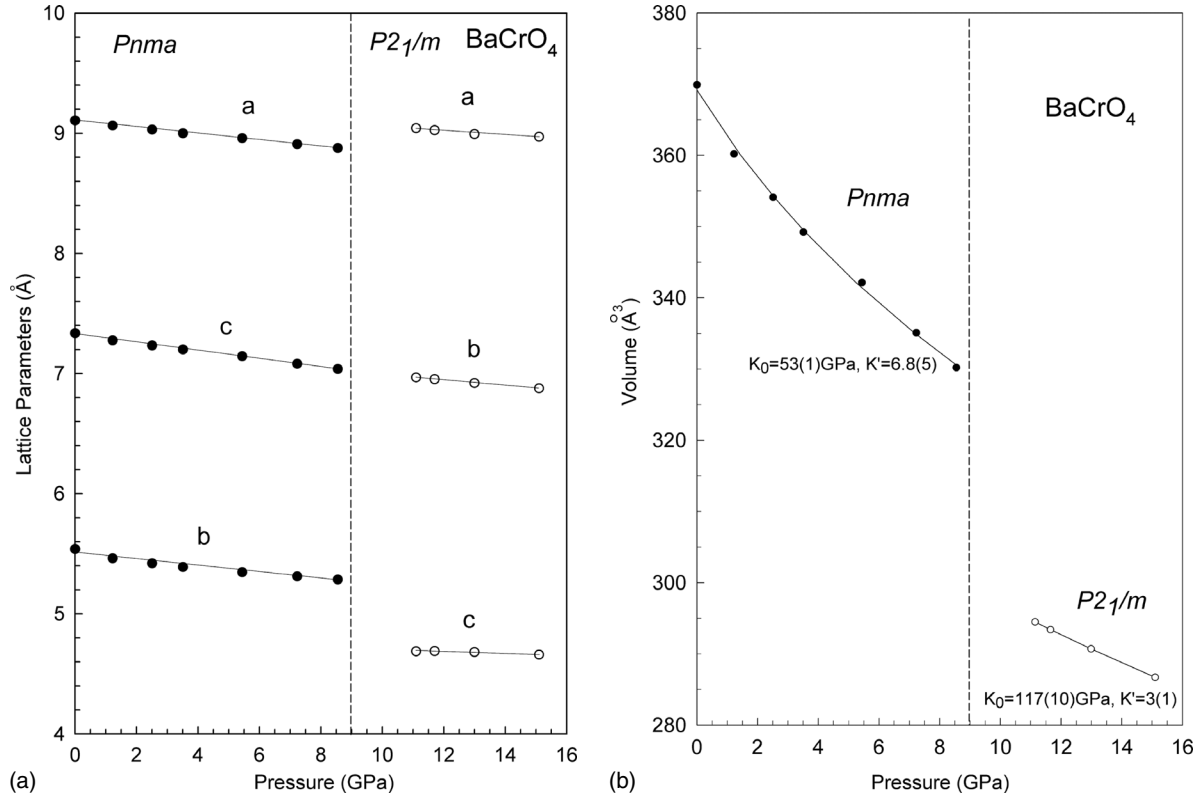

FIG. 6. (a) Comparisons of mean bond distances between CrO_4 and BaO_8 polyhedra to 9 GPa, (b) pressure dependence of Cr-O bond distances, and (c) pressure dependence of Ba-O bond distances.

TABLE II. Unit-cell lattice parameters a, b, c, volume V, linear compressibilities β_0, and bulk modulus K_0 of $BaCrO_4$ at different pressures.

P/GPa	a (Å)	b (Å)	c (Å)	V (Å^3)
0.0001	9.106(2)	5.539(1)	7.335(1)	369.92(7)
1.22(2)	9.064(2)	5.462(1)	7.276(1)	360.21(5)
2.51(5)	9.031(2)	5.420(1)	7.234(1)	354.11(5)
3.51(11)	9.000(2)	5.389(1)	7.200(1)	349.22(6)
5.44(13)	8.959(2)	5.346(2)	7.144(1)	342.14(8)
7.23(11)	8.909(6)	5.312(3)	7.081(3)	335.09(10)
8.55(10)	8.877(6)	5.285(3)	7.038(3)	330.20(11)
$\beta_0/10^{-3}$ GPa^{-1}	2.875	4.99	4.595	
K_0/GPa				53(1)

quencies of the compound. Considering the stretching frequencies of the high-pressure phase at 10.5 GPa (i.e., 892.2, 905.0, 927.8, and 943.1 cm^{-1}) we obtain the corresponding estimated Cr-O bond strengths of 1.57 v.u., 1.61 v.u., 1.68 v.u., and 1.74 v.u., respectively. With these numbers we can estimate a total valence of 6.6 for Cr that is approximated to the formal valence of 6. This verifies the configuration for the Cr ions in the high-pressure phase is still a tetrahedral configuration.

For barite ($BaSO_4$), the pressure for the phase transition found from x-ray diffraction data is 1–3 GPa higher than that of Raman data;[11] this difference is attributed to the superior sensitivity of Raman signals. For the intense Raman signals of $BaCrO_4$, the variations in Raman modes at the phase transition are readily detected and are thus more reliable. The Raman feature of the ν_1 mode of $BaCrO_4$ split into two peaks at pressure about 9 GPa (Figs. 4 and 5); for bending and lattice modes new peaks also emerged at a similar pressure, confirming the finding of a pressure-induced phase transformation and is consistent with the phase transition observed at about 9 GPa from our x-ray data. According to a combination of x-ray diffraction and Raman data, we conclude that a phase transition of $BaCrO_4$ occurs at near 9 GPa. Therefore, the phase-transition pressure of $BaSO_4$ is higher than that in $BaCrO_4$. Our results thus suggest that with increasing radius of the B-cation transition pressure decreased, in good agreement with Bastide's diagram. The Raman data show additional features at pressures greater than 9 GPa, indicating a distorted orthorhombic structure or a lower symmetry to be formed. Note that at least three new diffraction signals were found in our x-ray data. There are two possible explanations for the x-ray data finding; one is the coexistence of high- and low-pressure phases, and the other is the symmetry of the new high-pressure phase lower than orthorhombic. As our Raman data fail to support the former case, we conclude that the high-pressure form of $BaCrO_4$ above 9 GPa has either a distorted orthorhombic structure or even a structure of lower symmetry. To evaluate a possible solution for this high-pressure phase, we applied software DICVOL91 linked in the CRYSFIRE suite.[27] Eighteen diffraction lines of the high-pressure phase were indexed to monoclinic cells; these unit

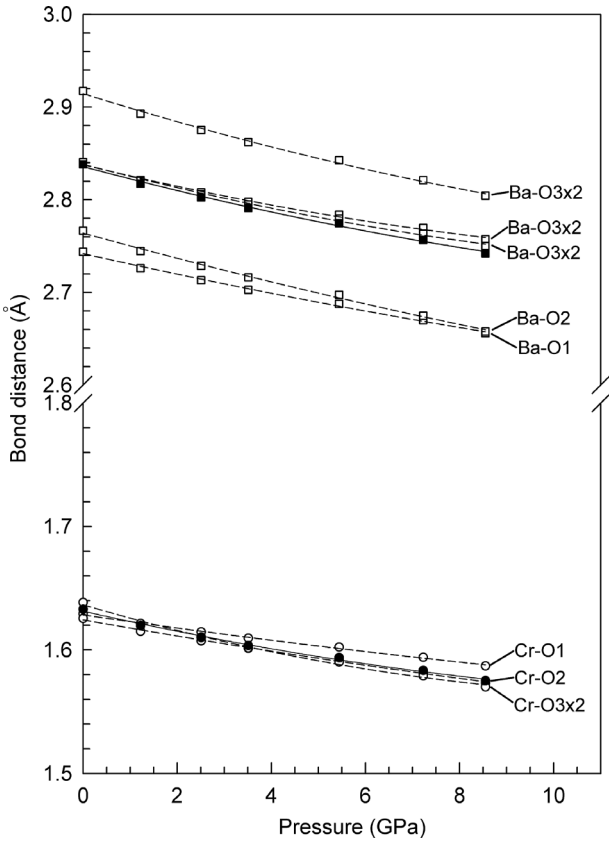

FIG. 7. (a) Pressure dependence of the lattice parameters of $BaCrO_4$ and (b) pressure dependence of the volume of $BaCrO_4$. Solid circles correspond to data for the barite phase and open circles for the high-pressure phase. The dashed line indicates the transition pressure.

cells, as given by the CRYSFIRE suite, were refined for the optimal space group with the aid of CHEKCELL software,[28] which indicated two monoclinic cells—space groups $P2_1$ and $P2_1/m$—with a figure of merit M(18)=5. We compared both $P2_1$ and $P2_1/m$ space groups and found $P2_1/m$ fitted our high-pressure diffraction data well. Furthermore, we also examined the $AgMnO_4$ phase ($P2_1/n$) for the high-pressure form of $BaCrO_4$ but the diffraction peak positions of $AgMnO_4$ phase failed to match our high-pressure phase of $BaCrO_4$. Therefore, $P2_1/m$ space group was adapted to our high-pressure form of $BaCrO_4$ and Le Bail method in GSAS program was thus used to obtain the lattice parameters. Our results showed that unit-cell lattice parameters of the high-pressure phase $BaCrO_4$-II at 11.1 GP are a=9.042(5) Å, b =6.968(2) Å, c=4.688(3) Å, and β=94.42(2)^0, together with other high-pressure data were listed in Table III and shown in Fig. 6(a). The volume data of the high-pressure phase $BaCrO_4$-II fitted to a third-order Birch-Murnaghan equation of state yielded a bulk modulus of 117(10) GPa and a pressure derivative of 3(1) [Fig. 6(b)]. In the structural transition from $BaCrO_4$ to $BaCrO_4$-II, the unit-cell volume decreases by about 9%.

V. CONCLUSION

Both our Raman and x-ray diffraction data of $BaCrO_4$ show a phase transition at about 9 GPa; the structure at am-

TABLE III. Unit-cell lattice parameters a, b, c, beta angle β, volume V, and bulk modulus K_0 of the high-pressure phase of $BaCrO_4$-II, at different pressures.

P/GPa	a (Å)	b (Å)	c (Å)	β (deg)	V (Å^3)
11.1(2)	9.042(5)	6.968(2)	4.688(3)	94.42(2)	294.5(1)
11.7(3)	9.025(5)	6.952(2)	4.690(3)	94.27(2)	293.4(1)
13.0(5)	8.993(6)	6.921(3)	4.682(4)	94.16(2)	290.7(2)
15.1(9)	8.971(7)	6.877(3)	4.660(4)	94.09(2)	286.7(2)
K_0/GPa					117(10)

bient pressure is proved to be recoverable. The structure of the high-pressure phase $BaCrO_4$-II is suggested to be a monoclinic $P2_1/m$ structure. This new high-pressure phase $BaCrO_4$-II is not included in the Bastide's diagram and may be the high-pressure form of other ABO_4-type compounds with orthorhombic *Pnma* structure. The distances of Ba-O (A cations) are more compressible than those of Cr-O (B cations) for $BaCrO_4$. In addition, for $BaCrO_4$ the b axis is the most compressible direction whereas the a axis is the least compressible one. The bulk modulus of $BaCrO_4$ calculated from the third-order Birch-Murnaghan equation of state is 53(1) GPa and its pressure derivative is 6.8(5), in agreement with theoretical calculations.[15] For the high-pressure phase $BaCrO_4$-II, the bulk modulus is determined as 117(10) GPa and its pressure derivative is 3(1).

ACKNOWLEDGMENTS

We thank J. Hu for her assistance in synchrotron x-ray data collections. Constructive comments from two anonymous reviewers and Sanda Botis improve the quality of this manuscript. National Science Council of Taiwan (Contracts No. NSC 96-2116-M-153-001, No. NSC 96-2628-M-006-003, No. NSC 97-2112-M-134-001-MY2, and No. NSC 97-2120-M-001-007) and Natural Sciences and Engineering Research Council of Canada provided support for this research.

[1] G. Voicu, M. Bardoux, and R. Stevensen, Ore Geol. Rev. **18**, 211 (2001).
[2] M. Nikl, P. Bohacek, N. Mihokova, N. Solovieva, A. Vedda, M. Martini, G. P. Pazzi, P. Fabeni, M. Kobayashi, and M. Ishii, J. Appl. Phys. **91**, 5041 (2002).
[3] A. Brenier, G. Jia, and C. Tu, J. Phys.: Condens. Matter **16**, 9103 (2004).
[4] M. Kobayashi, M. Ishi, Y. Usuki, and H. Yahagi, Nucl. Instrum. Methods Phys. Res. A **333**, 429 (1993).
[5] N. Faure, C. Borel, M. Couchoud, G. Basset, R. Templier, and C. Wyon, Appl. Phys. B: Lasers Opt. **63**, 593 (1996).
[6] O. Fukunaga and S. Yamaoka, Phys. Chem. Miner. **5**, 167 (1979).
[7] J. P. Bastide, J. Solid State Chem. **71**, 115 (1987).
[8] W. A. Crichton, J. B. Parise, S. M. Antao, and A. Grzechnik, Am. Mineral. **90**, 22 (2005).
[9] D. Errandonea and F. J. Manjón, Prog. Mater. Sci. **53**, 711 (2008).
[10] A. Lentz, W. Buchele, and H. Schollhorn, Cryst. Res. Technol. **21**, 827 (1986).
[11] P. L. Lee, E. Huang, and S. C. Yu, High Press. Res. **23**, 439 (2003).
[12] R. M. Hazen and L. W. Finger, *Comparative Crystal Chemistry* (Wiley, Chichester, 1982), pp. 151–164.
[13] R. M. Hazen, L. W. Finger, and J. W. E. Mariathasan, J. Phys. Chem. Solids **46**, 253 (1985).
[14] D. Errandonea, J. Pellicer-Porres, F. J. Manjón, A. Segura, Ch. Ferrer-Roca, R. S. Kumar, O. Tschauner, P. Rodríguez-Hernández, J. López-Solano, S. Radescu, A. Mujica, A. Muñoz, and G. Aquilanti, Phys. Rev. B **72**, 174106 (2005).
[15] U. Becker, P. Risthaus, F. Brandt, and D. Bosbach, Chem. Geol. **225**, 244 (2006).
[16] A. R. Patel and H. L. Bhat, J. Cryst. Growth **11**, 166 (1971).
[17] S. Klotz, J. C. Chervin, P. Munsch, and G. Le Marchand, J. Phys. D **42**, 075413 (2009).
[18] D. L. Heinz and R. Jeanloz, J. Appl. Phys. **55**, 885 (1984).
[19] H. K. Mao, J. Xu, and P. M. Bell, J. Geophys. Res. **91**, 4673 (1986).
[20] A. P. Hammersley, S. O. Svensson, M. Hanfland, A. N. Fitch, and D. Hausermann, High Press. Res. **14**, 235 (1996).
[21] A. C. Larson and R. B. Von Dreele, LANL Report No. 86-748, 2004 (unpublished).
[22] J. M. Alía, H. G. M. Edwards, A. Fernández, and M. Prieto, J. Raman Spectrosc. **30**, 105 (1999).
[23] L. Y. Chang, R. A. Howie, and J. Zussman, *Rock-Forming Minerals: Non-silicates*, 2nd ed. (Longman, Green, New York, 1996), Vol. 5B, pp. 4–38.
[24] Y. W. Long, L. X. Yang, S. J. You, Y. Yu, R. C. Yu, C. Q. Jin, and J. Liu, J. Phys.: Condens. Matter **18**, 2421 (2006).
[25] F. J. Manjón, D. Errandonea, N. Garro, J. Pellicer-Porres, P. Rodríguez-Hernández, S. Radescu, J. López-Solano, A. Mujica, and A. Muñoz, Phys. Rev. B **74**, 144111 (2006).
[26] B. M. Weckhuysen and I. E. Wachs, J. Chem. Soc., Faraday Trans. **92**, 1969 (1996).
[27] R. Shirley, The CRYSFIRE System for Automatic Powder Indexing: User's Manual (2002).
[28] J. Laugier and B. Bochu http://www.inpg.fr/LMPG